Critical Fracture Stress and Fracture Strain Models for the Prediction of Lower and Upper Shelf Toughness in Nuclear Pressure Vessel Steels

R. O. RITCHIE, W. L. SERVER, AND R. A. WULLAERT

Critical fracture stress and stress modified fracture strain models are utilized to describe the variation of lower and upper shelf fracture toughness with temperature and strain rate for two alloy steels used in the manufacture of nuclear pressure vessels, namely SA533B-1 (HSST Plate 02) and SA302B (Surveillance correlation heat). Both steels have been well characterized with regard to static and dynamic fracture toughness over a wide range of temperatures (−190 to 200°C), although valid J_{Ic} measurements at upper shelf temperatures are still somewhat scarce. The present work utilizes simple models for the relevant fracture micromechanisms and local failure criteria to predict these variations in toughness from uniaxial tensile properties. Procedures are discussed for modelling the influence of neutron fluence on toughness in irradiated steel, and predictions are derived for the effect of increasing fluence on the variation of lower shelf fracture toughness with temperature in SA533B-1.

DURING the operation of modern nuclear reactor plants, stringent pressure-temperature limitations for heat-up and cooldown of the reactor coolant system are imposed to provide adequate safety margins against the possibility of failure of the ferritic pressure vessel materials. Because of this concern over possible subcritical or critical fractures in the reactor vessel, a large research effort over the last decade has been directed at fully characterizing the toughness of nuclear pressure vessel steels as a function of alloy composition, residual element content, reactor operating temperature, and strain-rate in both unirradiated and neutron irradiated material.[1]

Nuclear pressure vessel steels, such as SA533B-1, undergo a classical fracture mode transition from low energy brittle fractures at low temperatures (lower shelf) to high energy ductile fractures at higher temperatures (upper shelf), as shown by the Charpy V-notch impact toughness data in Fig. 1.[2] This figure also indicates the marked degradation in toughness through a shift of the impact curve to higher temperatures from neutron irradiation. Fractographic observations[3] in such low strength steels have shown that, microscopically, low temperature (lower shelf) fractures occur by a transgranular cleavage mechanism along low energy cleavage planes, whereas at the upper shelf, fracture occurs by a mechanism of microvoid coalescence involving the initiation, growth and coalescence of small voids formed at inclusions, and second phase particles. Recently attempts have been made to relate these microscopic failure modes to the local mechanical criteria governing fracture, with the objective of describing macroscopic fracture toughness behavior. Failure at the lower shelf has been modeled as slip-initiated cleavage fracture using the critical stress criterion proposed by Ritchie, Knott, and Rice (RKR).[4] Failure at the upper shelf has been modeled as microvoid coalescence using a stress modified strain criterion originally proposed by McClintock[5] and adapted by MacKenzie and coworkers.[6] Successful application of such models requires a determination of critical fracture stress and strain values from notched bend and tensile tests and a knowledge of precise analyses for the elastic-plastic stress and strain distributions ahead of sharp cracks, together with an evaluation of the microstructurally significant size-scales governing fracture.

The present studies were instigated to determine the feasibility of applying such simple models to predict the variation of both lower and upper shelf static and dynamic fracture toughness with temperature and strain-rate for two ferritic alloy steels utilized in the construction of nuclear pressure vessels, namely SA533B-1 and SA302B. The work constitutes an extension of studies by Parks[7] who showed the applicability of the RKR model to describe lower shelf static toughness in SA533B-1. Further, procedures are developed for determining the influence of increasing neutron fluence on toughness in irradiated steel, and predictions are derived for lower shelf fracture toughness in irradiated SA533B-1.

FRACTURE MODELS

Critical Stress Model for Lower Shelf Toughness

Early studies of slip-initiated low temperature cleavage fracture for Mode I loading in mild steel indicated that cleavage cracks propagate in an unstable manner when the maximum principal (tensile) stress (σ_{yy}) ahead of a stress concentrator exceeds a critical value (σ_f^*), which is relatively independent of both temperature and strain-rate.[8,9] This critical stress criterion for cleavage fracture predicts failure to be

R. O. RITCHIE is Associate Professor, Department of Mechanical Engineering, Massachusetts Institute of Technology, Cambridge, MA 02139. W. L. SERVER and R. A. WULLAERT are Vice President and President, respectively, Fracture Control Corporation, Goleta, CA 93017.

Manuscript submitted March 5, 1979.

ISSN 0360-2133/79/1011-1557$00.75/0

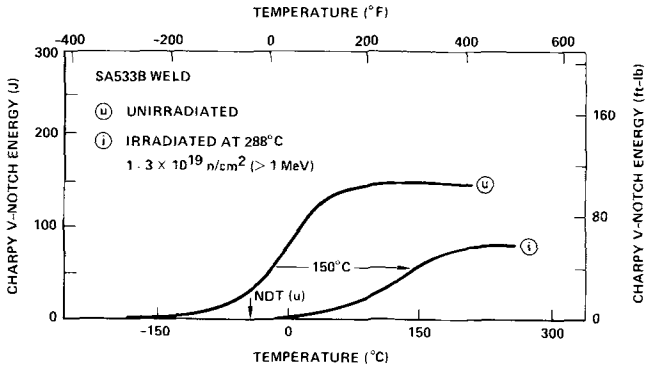

Fig. 1—Variation of Charpy V-notch impact toughness with temperature for unirradiated (u) and irradiated (i) SA533B-1, taken from a weld in the beltline region of the pressure vessel in the Maine Yankee Nuclear Reactor[2].

dependent on the degree of work hardening and yield strength in achieving high local tensile stresses. With the advent of precise elastic-plastic stress distributions ahead of sharp cracks, namely the asymptotic HRR crack tip singularity of Hutchinson,[10] and Rice and Rosengren,[11] subsequent finite element solutions,[12,13] and the near-tip stress and strain alterations due to finite geometry changes involved in progressive crack tip blunting,[14,15] it became possible to relate such local failure criteria to macroscopic fracture behavior, as described by fracture toughness K_{Ic}. The RKR model[4] proposes a local criterion for unstable slip-initiated cleavage ahead of *sharp cracks* which requires the local tensile stress (σ_{yy}) to exceed a critical fracture stress (σ_f^*) over a microstructurally significant characteristic size-scale (l_o^*). Accordingly, the low temperature fracture toughness can be related to the material's yield and fracture stresses. RKR derived quantitative predictions of the variation with temperature of the cleavage fracture toughness in mild steel using a characteristic distance of the order of two ferritic grain diameters.[4] Other workers have since demonstrated the applicability of this model to failure in low alloy steels,[7] higher carbon steels,[16] and mild steel over a range of grain sizes,[17,18] and titanium alloys.[19]

The model can be formulated analytically[18] by considering the HRR small scale yielding solution for the plane strain tension stress distribution around a stationary crack tip in a nonlinear elastic material.[10] Using the Ramberg-Osgood constitutive law, in which the plastic strain ($\bar{\epsilon}^p$) as a function of equivalent stress ($\bar{\sigma}$) is given by $\bar{\epsilon}^p = \epsilon_o(\bar{\sigma}/\sigma_o)^N$, the normal stress at distance x *directly* ahead of the crack tip (σ_{yy}) is:

$$\frac{\sigma_{yy}}{\sigma_o} = f(N)\left(\frac{J}{\epsilon_o I\, x}\right)^{1/(N+1)} \qquad [1]$$

where σ_o is the flow stress, J the J contour integral[20] to which the crack is loaded, ϵ_o the yield strain, N the Ramberg-Osgood hardening exponent, I a numerical constant weakly dependent on N, and $f(N)$ the value, directly ahead of the crack, of the normalized angular distribution of σ_{yy}. By expressing Eq. [1] in terms of the linear elastic stress intensity K and taking σ_o as the initial tensile yield stress, this becomes:

$$\frac{\sigma_{yy}}{\sigma_y} = f(N)\left[\frac{(1-\nu^2)}{\epsilon_o I}\right]^{1/(N+1)}\left[\frac{x}{(K/\sigma_y)^2}\right]^{-1/(N+1)} \qquad [2]$$

By applying the RKR criterion that $K = K_{Ic}$ when σ_{yy} exceeds σ_f^* over a characteristic distance $x = l_o^*$ directly ahead of the crack tip, an expression for the fracture toughness is obtained,

$$K_{Ic} = \beta^{-((N+1)/2)}\, l_o^{*1/2}\left[\frac{\sigma_f^{[(N+1)/2]}}{\sigma_y^{[(N-1)/2]}}\right] \qquad [3]$$

where,

$$\beta = f(N)\left[\frac{(1-\nu^2)}{\epsilon_o I}\right]^{1/(N+1)} \qquad [3a]$$

is the amplitude of the stress singularity. Typical values of I, $f(N)$, and β as a function of hardening exponent are listed in Table I.*

*It should be noted that Eq. [3] is presented as one representation of the analytical form of the RKR model, since it is based solely on the HRR asymptotic crack tip singularity, and correspondingly does not reflect the refinements in the stress distribution derived from more recent finite element solutions,[12,13] or the near-tip alterations due to crack tip blunting.[14,15] Application of the model is thus best achieved by reference to these specific solutions.

Experimental determination of critical fracture stress (σ_f^*) values is achieved by fracturing V-notched bend bars at low temperatures.[4,9,17,21,22] Traditionally the value of σ_f^* has been calculated from slip-line field theory to determine the maximum local tensile stress (σ_{yy}^{max}) at the notch root at failure. Where fracture loads are well below general yield, Hill's exponential spiral slip-line solution has been used,[21,22] namely:

$$\sigma_{yy}^{max} = 2k[1 + \ln(1 + r_y^c/\rho)] \qquad [4]$$

where k is the shear yield stress, ρ is the notch root radius, and r_y^c is the critical plastic zone size dimension.[23] Alternatively, by determining the temperature at which fracture is coincident with general yield for different notch flank angles (θ), the Green and Hundy solution[24] has been employed where:

$$\sigma_{yy}^{max} = 2k[1 + \pi/2 - \theta/2], \text{ for } \theta \geq 6.4 \text{ deg.} \qquad [5]$$

More recently, however, Griffiths, Owen, and coworkers[25,26] have derived accurate finite element solutions for the elastic-plastic stress distributions in V-notched four-point bend specimens for hardening materials, and the determination of σ_f^* is now best achieved using such analyses.[17]

Thus, use of the RKR model[4] for predicting the temperature variation of lower shelf fracture toughness involves determining σ_f^*, together with the variation of

Table I. Numerical Values of I, f(N) and β for HRR Small Scale Yielding Solution for Plane Strain Tension Stress Distribution Directly Ahead of the Crack Tip (Eqs. [1] to [3])

Hardening Exponent N	I	$f(N)$	β^1
$N = 3$	5.51	1.94	5.50
$N = 5$	5.02	2.22	4.52
$N = 9$	4.60	2.46	3.80
$N = 13$	4.40	2.58	3.53
$N = 25$	4.14	2.73	3.24
$N = 49$	3.96	2.83	3.10
$N = 99$	3.84	2.90	3.03

[1] Computed for $\nu = 0.33$ and $\epsilon_o = 0.0025$, typical of a low strength steel

rected for the estimated crack tip strain-rates), and employing a suitable characteristic distance representative of the microstructure and fracture micromechanisms involved. For low temperature slip-initiated cleavage fracture, this characteristic distance has been generally found to be some small multiple of the grain size [4,7,16-18,22] and most probably represents the distance from the crack tip where the first grain boundary carbide initiates catastrophic failure.[4]

Critical Strain Model for Upper Shelf Toughness

Metallographic studies[3] of the mechanisms of fracture of nuclear pressure vessel steel, *i.e.*, SA533B-1, at temperatures corresponding to the upper shelf, reveal that dimpled rupture initiates by void nucleation and growth at large manganese sulfide and aluminum oxide inclusions (5 to 10 μm in size) ahead of the crack tip. The subsequent growth of such voids becomes limited by a plastic shear instability between neighboring voids and the main crack tip, the linkage constituting crack growth. This instability is due to a localization of strain between large voids and occurs by a fine scale coalescence of microvoids ("void sheets") nucleated at submicron (~1/2 μm) iron carbide particles.

One can realistically model such ductile fracture as being strain induced, in that macrocrack growth via linking of voids occurs when some critical strain is exceeded ahead of the crack tip. However, as McClintock[5] first pointed out, void growth during ductile fracture is also a strong function of stress state, *i.e.*, the ratio of mean to equivalent flow stress. Furthermore, in an analogous situation to cleavage fracture,[4] it is not sufficient for the failure criterion for ductile fracture to simply involve a critical strain to be reached at a single point ahead of the crack tip, but rather for this strain to be everywhere exceeded over a minimum amount of material which is characteristic of the scale of physical events involved. Accordingly, MacKenzie and coworkers[6] have proposed a criterion for ductile failure where a critical fracture strain ($\bar{\epsilon}_f^*$) is locally exceeded over some microstructurally significant characteristic distance (l_o^*) ahead of the crack tip, but which further recognizes that this critical strain is a strong function of stress state which itself varies with distance ahead of the crack tip.

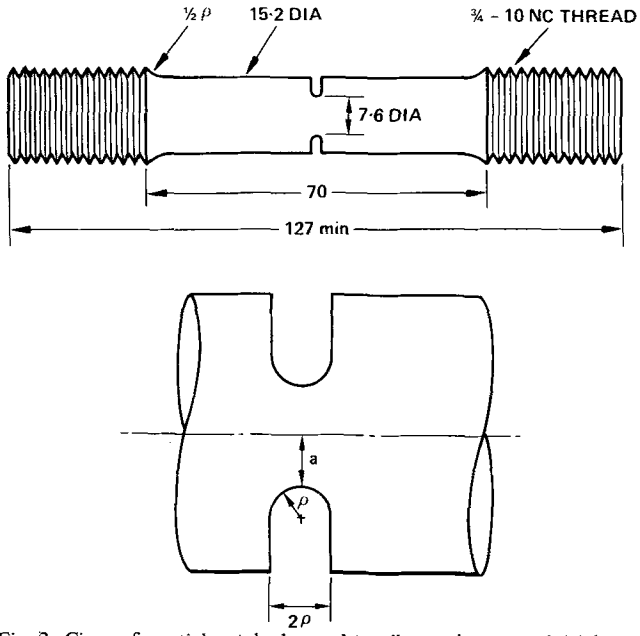

Fig. 2–Circumferential notched round tensile specimen. a_0, initial radius of notched cross section = 3.8 mm, ρ, notch root radius, tested at values of 1.27, 1.91, 2.54, 3.81, and 6.35 mm. All dimensions in mm.

The application of this stress modified strain model for the prediction of upper shelf fracture toughness involves experimental determination of the fracture strain ($\bar{\epsilon}_f$) or ductility as a function of stress state, together with knowledge of the elastic-plastic strain distribution ahead of a sharp crack. Values of $\bar{\epsilon}_f$ can be obtained using circumferentially notched round tension specimens loaded uniaxially (Fig. 2), where different states of stress are achieved by varying the notch acuity.[6,27] Using the standard definitions of equivalent stress ($\bar{\sigma}$), mean or hydrostatic stress (σ_m) and equivalent plastic strain ($\bar{\epsilon}_p = \int d\bar{\epsilon}_p$), the Bridgeman analysis for the necked tensile specimen[29] gives a constant strain distribution at the minimum cross-section of:

$$\bar{\epsilon}_p = \int d\bar{\epsilon}_p = 2 \ln \frac{a_o}{a_{\min}}, \qquad [6]$$

for a stress state at the center of the specimen of:

$$\sigma_m/\bar{\sigma} = 1/3 + \ln\left(1 + \frac{a_{\min}}{2\rho}\right), \qquad [7]$$

where ρ is the notch root radius and a_o and $a_{\min}$ are the original and minimum radii of the notched cross-section respectively (Fig. 2). By loading a series of such specimens with varying ρ under notch opening displacement control, values of $\bar{\epsilon}_p$ at failure initiation ($\bar{\epsilon}_f$) are obtained as a function of $\sigma_m/\bar{\sigma}$. The distribution of strain ($\bar{\epsilon}_p$) and stress state ($\sigma_m/\bar{\sigma}$) ahead of a crack tip for small scale yielding are then taken from the blunting solutions of Rice and Johnson[14] or McMeeking[15] as a function of distance ahead of the crack (x) normalized with respect to crack tip opening displacement δ (Fig. 3). Fracture toughness values are now predicted by determining the value of δ for which the equivalent plastic strain ($\bar{\epsilon}_p$) exceeds, over the characteristic distance (l_o^*), the value of critical fracture strain (ϵ_f^*) representative of the crack tip stress state at that position. Thus, if the small scale yielding strain distribution[14,15] is written in the form;[31]

$$\bar{\epsilon}_p = c_1 \frac{\delta}{x} \qquad [8]$$

where c_1 is a constant determined from Fig. 3, then at initiation of ductile fracture, $\bar{\epsilon}_p = \bar{\epsilon}_f^*$ at distance $x = l_o^*$ when $\delta = \delta_c$. K_{Ic} values may be related to the critical crack tip opening displacements (δ_c) using the small scale yielding formulation:[30]

$$\delta_c = 0.6 \frac{K_{Ic}^2}{E\sigma_y} \qquad [9]$$

where E is the elastic modulus and σ_y the yield strength. By combining Eqs. [8] and [9], the critical strain model can be expressed in the form:[31]

$$K_{Ic} = \text{constant} \sqrt{\bar{\epsilon}_f^* \cdot l_o^* \cdot \sigma_y \cdot E} \ . \qquad [10]$$

Since the failure event for ductile fracture generally

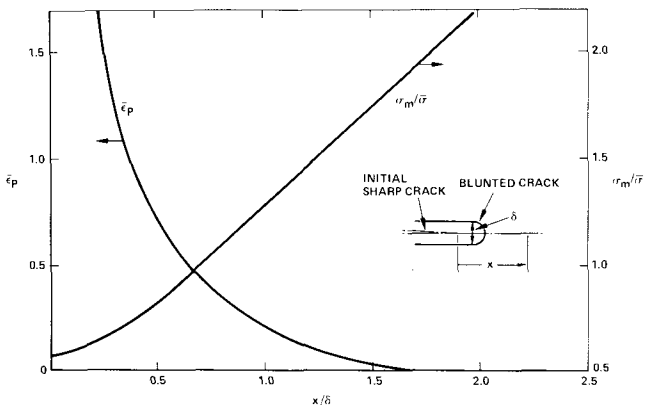

Fig. 3—Distribution of plastic strain ($\bar{\epsilon}_p$) and stress state ($\sigma_m/\bar{\sigma}$) near crack tip, from Rice and Johnson small scale yielding solution.[14]

involves coalescence by shear localization between a number of voids nucleated at the largest particles, values of l_o^* for such fracture are generally found to be some small multiple of the interparticle spacing.[5,6,16,27,31]

MATERIALS AND EXPERIMENTAL PROCEDURES

Materials and Microstructure

The materials examined were two low strength alloy steels utilized in nuclear pressure vessel construction, namely the currently used material SA533 Grade B Class 1 (HSST Plate 02) and the formerly used material SA302B (Surveillance correlation heat). The composition and standard mechanical properties of these

Table II. Composition in Weight Percent of Nuclear Pressure Vessel Steels

Material	Heat Code	Chemistry in Weight Percent									
		C	Mn	P	S	Si	Ni	Cr	Mo	V	Cu
SA533B-1 (HSST Plate 02)	1bA	0.23	1.55	0.009	0.014	0.20	0.67	0.04	0.53	0.003	0.16
SA302B (Surveillance correlation heat)	4bA	0.23	1.47	0.013	0.024	0.26	0.17	0.05	0.52	0.004	0.20

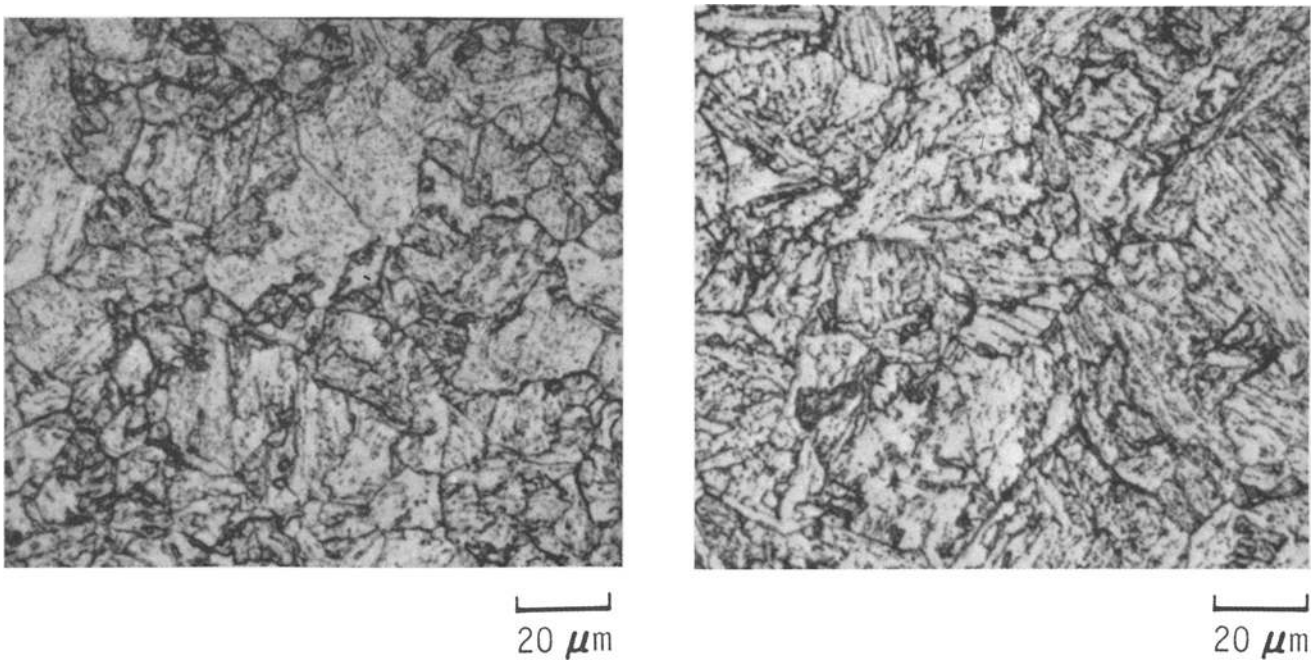

(a) (b)

Fig. 4—Optical microstructures of (*a*) SA533B-1 (HSST plate 02) and (*b*) SA302B (Surveillance correlation heat) showing predominately tempered bainitic structure.

Table III. Mechanical Properties of Nuclear Pressure Vessel Steels (T–L Orientation)

Material	Heat Code	Tensile Properties at 24°C			NDTT	Charpy V-Notch Energy, Upper Shelf
		Yield Stress, MPa	UTS, MPa	Elongation*, Pct	°C	J
SA533B-1	1bA	481	642	25.4	−29	137
SA302B	4bA	465	625	25.2	−18	60

*For 50.8 mm gage length.

steels are shown in Tables II and III, respectively.

Both materials were received in the heat treated condition which consisted of:

SA533B-1 – Normalized 4 h at 914°C, air cooled, austenitized 4 h at 900°C, agitated water quenched,
Tempered 4 h at 664°C, water quenched,
Stress relieved 40 h at 612°C, furnace cooled.

SA302B – Austenitized 4 h at 900°C, water quenched,
Stress relieved 6 h at 650°C, air cooled.

As with many low alloy steels quenched or normalized in thick section plate, the microstructure of both steels (Fig. 4) is primarily acicular tempered upper bainite with a small volume fraction of proeutectoid ferrite.* Prior austenite grain sizes ($\bar{d}$) were measured at 25 μm for SA533B-1 and 33 μm for SA302B. Although extensively investigated with respect to mechanical properties, there is a surprising lack of information in the literature with regard to the fine scale microstructures of these steels. Particle morphology and distribution, however, has been studied by Van Stone[3] in a similar plate of SA533B-1, indicating around 0.12 vol pct of manganese sulfide and aluminum oxide inclusions (5 to 10 μm in size) with equiaxed submicron cementite precipitates (1/2 μm in size) in bands along bainitic laths. No information could be found on the fine scale microstructural details of SA302B, except that deduced from fracture morphology.

*It is not possible from optical microscopy to make a clear distinction, but certain studies on HSST Plate 01 of SA533B-1 claim that the blocky ferritic areas are actually granular bainite since they contain evidence of carbide precipitation.[32]

Table IV. Measured Values of Critical Cleavage Fracture Stress (σ_f^*) for Nuclear Pressure Vessel Steels.

Material	Critical Cleavage Fracture Stress (σ_f^*)	
	Static, MPa	Dynamic Impact, MPa
SA533B-1	1830	2000
SA302B	1650	1900

Mechanical Properties

Both steels, particularly SA533B-1, have been the subject of extensive mechanical property characterization by the United States Atomic Energy Commission Heavy Section Steel Technology (HSST) Program[1] and the Electric Power Research Institute (EPRI) Programs.[33] In particular, a large volume of data now exists for the variation of strength and toughness with temperature and strain-rate in unirradiated and irradiated material as a function of plate position, orientation and heat-to-heat variations. The present study was focused on HSST Plate 02 of SA533B-1 (EPRI designated heat 1bA) and the Surveillance Correlation Heat of SA302B (EPRI designated heat 4bA) in the T-L orientation at plate positions between quarter and center thickness.

Fracture toughness data were obtained primarily from the EPRI Data Bank on nuclear pressure vessel steels.[33] ASTM valid static fracture toughness, K_{Ic}, data for the T-L orientation in unirradiated SA533B-1 were obtained from slow bend precracked Charpy and 1 in. (25.4 mm) thick compact (termed 1-T) test pieces over the temperature range of −196 to 0°C. The rate of loading for such data was consistent with an increase in stress intensity $\dot{K}$ of ~3 MN · m$^{-3/2}$ · s^{-1}, representing an approximate crack tip strain-rate of 10^{-2}s^{-1}. In addition, upper shelf values at temperatures between 0 and 200°C were computed from valid elastic-plastic J_{Ic} tests on 1-T compacts using the multi-specimen R-curve procedure for defining crack initiation,[34] where:

$$K_{Ic} \simeq K_{Jc} = \sqrt{J_{Ic}E/(1-\nu^2)} \qquad [11]$$

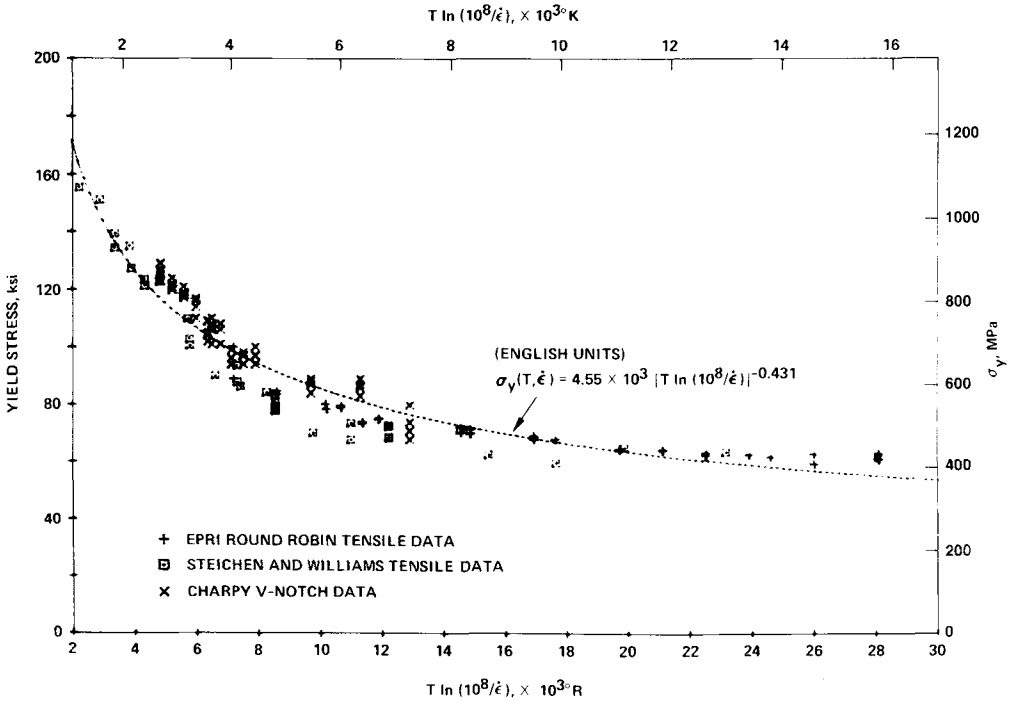

Fig. 5—Yield stress data for unirradiated SA533B-1 normalized by the rate-temperature parameter $T\ln(10^8/\dot{\epsilon})$. Data from Refs. 38 to 41.

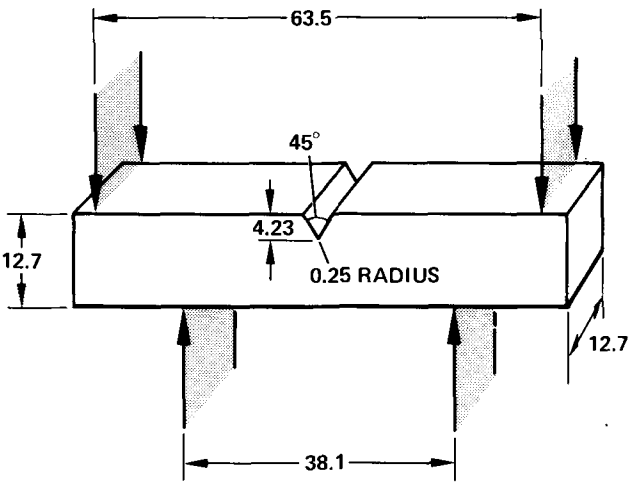

Fig. 6—Schematic diagram of V-notched four-point bend specimen for measurement of σ_f^*. All length dimensions are in units of mm.

where K_{Jc} is the value of K_{Ic} computed from J_{Ic}, E is the elastic modulus, and ν is Poisson's ratio. Additional lower shelf K_{Ic} data were acquired from the reports of the HSST programs on Plate 02 in the L-T orientation, obtained from valid tests using 1 in. (25.4 mm) to 11 in. (280 mm) thick (1T-11T) compact test pieces.[35-38] Dynamic fracture toughness (K_{Id}) was also examined at lower shelf temperatures between −140 and 0°C for two stress intensity rates $\dot{K}$ of 10^3 to 10^4 and 10^5 MN · m$^{-3/2}$ · s^{-1}. K_{Id} data for $\dot{K} = 10^3$ to 10^4 MN · m$^{-3/2}$ · s^{-1}, representing an approximate crack tip strain-rate $\dot{\epsilon}$ of 5 s^{-1}, were taken from the EPRI Data Bank[33] for 1-T to 4-T dynamic compact tests in the T-L orientation. K_{Id} data for $\dot{K} = 10^5$ MN · m$^{-3/2}$ · s^{-1} ($\dot{\epsilon} \simeq 3 \times 10^2$ s^{-1}) were taken from the same source[33] for instrumented precracked Charpy impact and dynamic 1-T band tests on the T-L orientation. Additional valid K_{Id} data at $\dot{K} = 10^5$ MN · m$^{-3/2}$ · s^{-1} were obtained from the HSST Program[35] for 1-T compact tests in the L-T orientation.

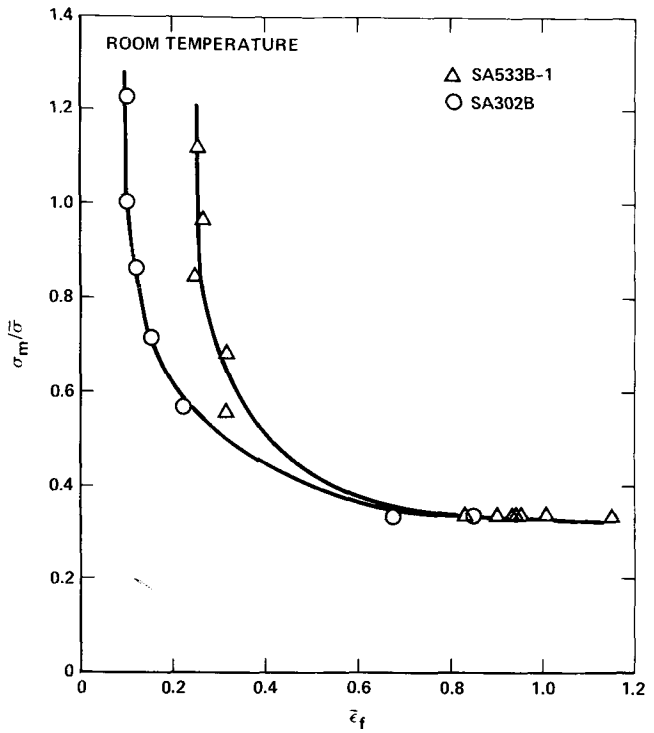

Fig. 7—Failure initiation curves for changing stress state at room temperature (24°C).

Toughness data on unirradiated SA302B were scarce. Valid static fracture toughness K_{Ic} ($\dot{\epsilon} \simeq 10^{-2}$ s^{-1}) values between −130 and 200°C on the T-L orientation were obtained from slow bend precracked Charpy and 1-T compact tests.[33] Valid dynamic fracture toughness K_{Id} ($\dot{\epsilon} \simeq 3 \times 10^{-2}$ s^{-1}) at lower shelf temperatures (−150 to 0°C) for the T-L orientation were obtained from instrumented precracked Charpy impact and dynamic 1-T bend tests.[33]

Tensile yield strength data for both steels in the unirradiated condition were taken from the EPRI Data Bank,[33] and Refs. 38 to 41. Additional high strain-rate data were derived from measurements of the general yield load on V-notch and precracked Charpy impact tests.[41] Yield stress (σ_y) data as a function of temperature and strain-rate were compiled, using the strain-rate temperature relationship of Bennett and Sinclair,[42] in terms of $T \ln(A/\dot{\epsilon})$, where T is the absolute temperature, $\dot{\epsilon}$ the strain-rate, and A a constant equal to 10^8 s^{-1} (Fig. 5). For prediction of fracture toughness values from such uniaxial data, yield stress values were corrected for approximate crack tip strain-rates; that is $\dot{\epsilon} \simeq 10^{-2}$ s^{-1} for static tests, $\dot{\epsilon} \simeq 5$ s^{-1} for dynamic compact tests, and $\dot{\epsilon} \simeq 3 \times 10^2$ s^{-1} for dynamic (impact) tests.

Experimental Determination of Critical Fracture Stress and Strain (σ_f^*, $\bar{\epsilon}_f^*$)

Critical fracture stress (σ_f^*) values for lower shelf slip initiated cleavage in both unirradiated SA533B-1 and SA302B were determined from slow bend and impact four-point bend tests on 45 deg V-notched bars (Fig. 6) broken at temperatures of −73, −129, and −193°C, where failure occurred catastrophically by unstable cleavage well before general yielding. Slow bend tests were performed at an effective crack tip strain-rate of approximately 10^{-4} s^{-1}, and impact tests were performed at $\dot{\epsilon} \simeq 50$ s^{-1}. The nominal bending stress at the onset of catastrophic failure was measured in each test, and using the Griffith and Owen[25] finite element stress distribution for this particular geometry of test piece, the critical values of the maximum principal stress at the crack tip ($\sigma_{yy}^{max} = \sigma_f^*$) were computed (Table IV).*

*Values of yield stress used in the computation were corrected for the particular crack tip strain-rates, as described above.

Fracture strain ($\bar{\epsilon}f$) values as a function of stress state ($\sigma_m/\bar{\sigma}$) for upper shelf ductile fracture in both steels were determined from circumferentially notched tensile tests at 24, 71, and 177°C. Unnotched and notched test pieces (Fig. 2) with root radii ρ of 1.27, 1.91, 2.54, 3.81, and 6.35 mm were loaded under longitudinal displacement control, monitored with an axial strain transducer mounted across the notch. In addition, a diametral strain transducer was mounted in the notch to continuously monitor changes in the minimum diameter of the notched cross-section. Failure initiation was defined as the point when the average axial stress (applied load divided by instantaneous cross-sectional area) dropped sharply prior to final failure. The fracture strain ($\bar{\epsilon}_f$) was computed as the equivalent plastic strain ($\bar{\epsilon}_p$) at this

point using Eq. [6]. The corresponding stress state $\sigma_m/\bar{\sigma}$ at the center of the neck where failure initiated was determined using Eq. [7]. Plots of fracture strain ($\bar{\epsilon}_f$) *vs* stress state ($\sigma_m/\bar{\sigma}$) for both materials at room temperature, 71°C and 177°C are shown in Figs. 7 to 9, and clearly indicate the marked reduction in ductility as the hydrostatic stress state is increased. Further, it can be seen that whereas both steels show similar ductility values in uniaxial tension ($\sigma_m/\bar{\sigma}$ = 1/3), at highly triaxial stress states (*i.e.*, $\sigma_m/\bar{\sigma}$ = 1.2) SA302B shows a significantly smaller fracture strain.

The critical fracture strain ($\bar{\epsilon}_f^*$), used to predict fracture toughness and representing material ductility ahead of a crack tip, was taken as the value of $\bar{\epsilon}_f$ corresponding to the particular stress state at the characteristic distance from the crack tip (from Fig. 3). For the cases studied, this corresponded to the fracture strain at values of $\sigma_m/\bar{\sigma}$ in excess of 1.2

Estimation of Characteristic Distances (l_o^*)

Precise determination of the critical microstructural size scale for either cleavage or ductile fracture demands at least that the complete micromechanisms of failure are fully understood. Since the local mechanisms of critical failure events in these steels are not known, it would be impossible from first principles to determine these characteristic distances. In their derivation of the critical stress model for cleavage fracture, RKR[4] found best agreement with experimental data with a characteristic distance of two ferrite grain diameters ($l_o^* \simeq 2\bar{d}$ = 120 μm) in mild steel, but there is no real fundamental physical significance for this. In fact, as Parks[7] states, "the dimension must be regarded as essentially an empirically obtained quantity, though presumably of relevance to microstructural aspects of fracture initiation."

However, examination of lower shelf cleavage fractures in SA533B-1 and SA302B (Fig. 10) reveals that cleavage facets are of the order of the prior austenite grain size rather than, say, the bainite packet size. Further, it is not unreasonable to presume that the critical fracture event is either the cracking of a grain boundary carbide or the propagation of the matrix crack through the next grain boundary, *i.e.*, occurring over the first few prior austenite grains from the crack tip. Accordingly for lower shelf toughness predictions characteristic distances were chosen between $2\bar{d}$ and $4\bar{d}$ with $\bar{d}$, the prior austenite grain size, measured as 25 and 33 μm for SA533B-1 and SA302B, respectively, consistent with previous estimates by Parks.[7]

At upper shelf temperatures, the initiation event for ductile fracture, where the displacements produced by internal necking between particles are critical, would not be possible over distances smaller than particle spacing. Since in the present steels it is the linkage by shear localization between large voids, nucleated at inclusions, which describes the initiation of actual ductile crack growth,[3] a lower bound estimate of the characteristic distance must be the inclusion spacing. Examination of upper shelf fractures in both steels (Fig. 11) shows that the spacing between major voids on fracture surfaces is roughly 50 μm in SA533B-1 (consistent with previous inclusion distribution studies[3]) and 100 to 150 μm in SA302B.

PREDICTION OF UNIRRADIATED TOUGHNESS

Lower Shelf Toughness

The temperature dependence of static fracture toughness (K_{Ic}) at the lower shelf for unirradiated SA533B-1 steel, between −200 and 0°C, is illustrated in Fig. 12, together with calculated values, determined from the RKR critical cleavage stress model[4] for characteristic distances of 2, 3, and 4 prior austenite

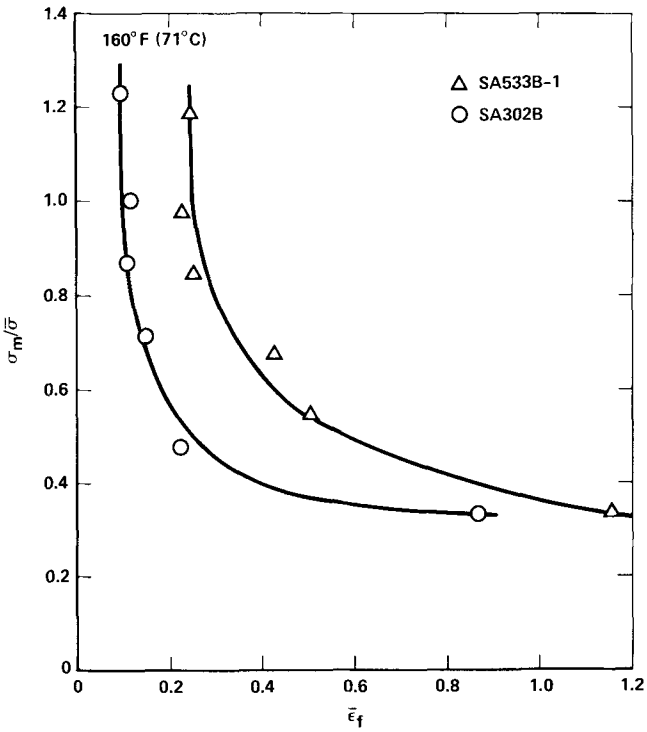

Fig. 8—Failure initiation curves for changing stress state at 71°C.

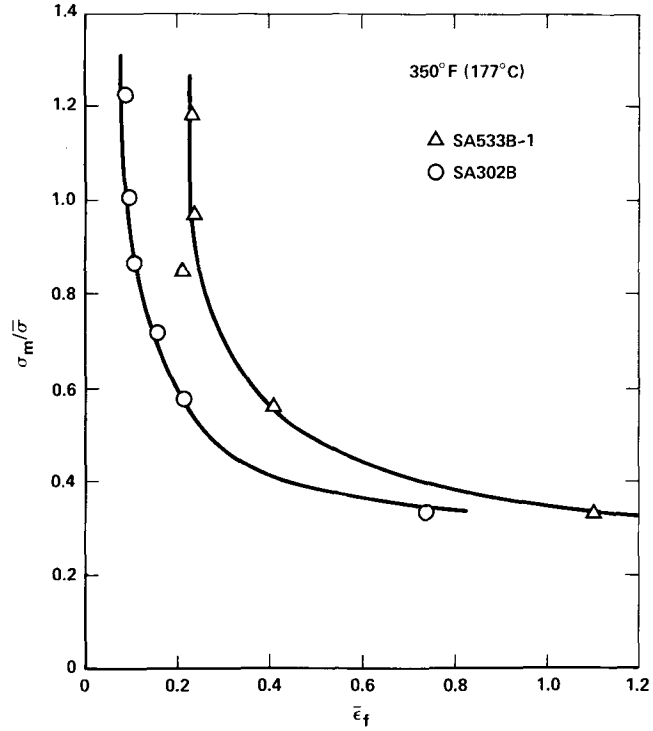

Fig. 9—Ductile failure initiation curves for changing stress state at 177°C.

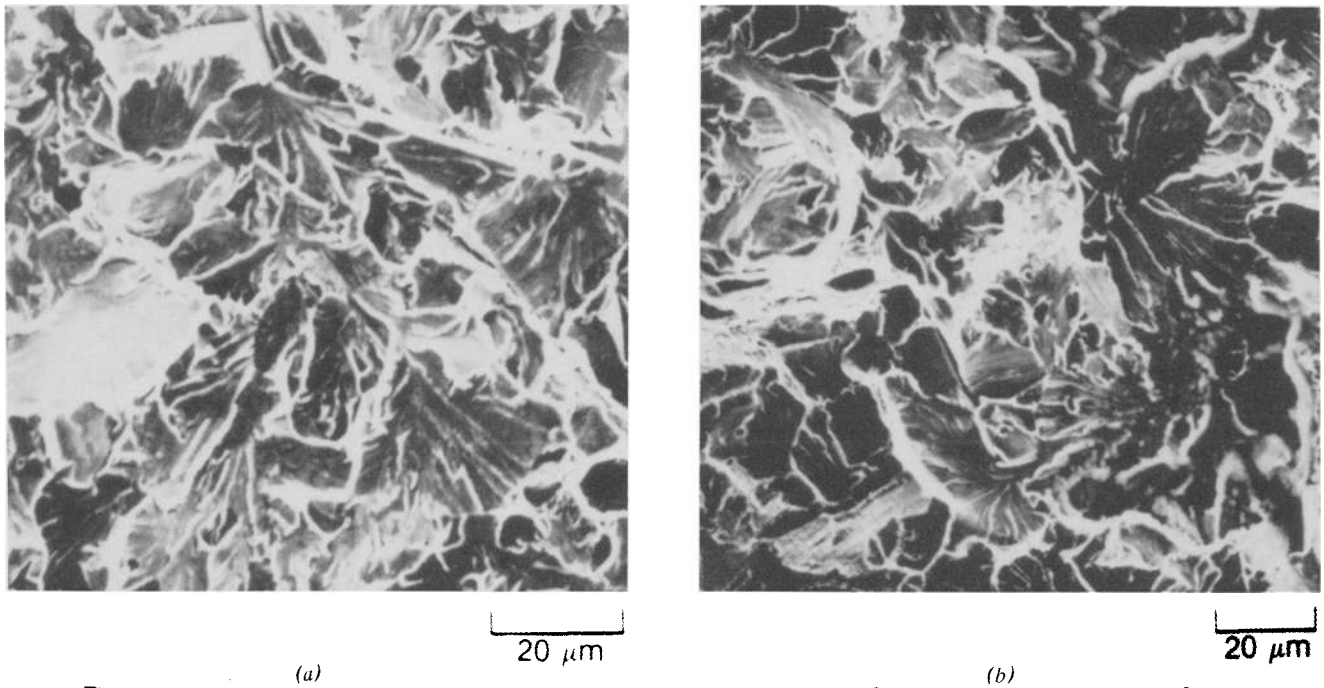

(a) (b)

Fig. 10—Transgranular cleavage fractures at lower shelf for (*a*) SA533B-1 tested at −78°C, and (*b*) SA302B tested at −68°C.

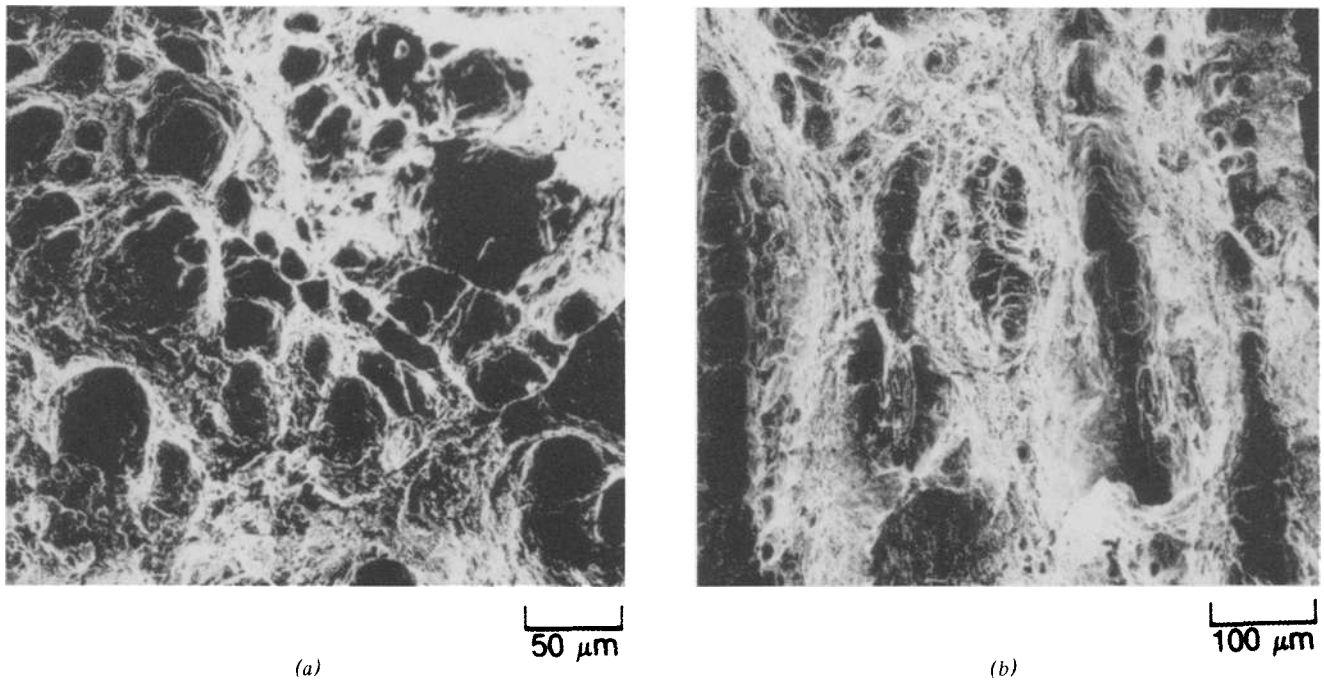

(a) (b)

Fig. 11—Ductile fracture by microvoid coalescence at upper shelf for (*a*) SA533B-1 and (*b*) SA302B tested at 71°C.

grain diameters. Predictions are based on the temperature dependence of yield strength shown in Fig. 5 calculated for approximate crack tip strain-rates of 10^{-2} s^{-1}, a criitcal cleavage stress σ_f^* of 1830 MPa (Table IV) assumed independent of temperature, a work hardening exponent n of 0.1 (N = 10)* representing an average value for this steel over the temperature range −200 to 0°C, and plane strain crack tip stress analyses due to Rice and Tracy[12,13] (finite element power law hardening solution) and Rice and Johnson[14] (approximate near-tip solution due to blunting for an initial yield strain of 0.0025). Similar predictions for the temperature variation of lower shelf dynamic fracture toughness (K_{Id}) of unirradiated SA533B-1 are shown in Figs. 13 and 14 for approximate crack tip strain-rates of 5 and 3×10^2 s^{-1}, respectively. Results for lower shelf static and impact fracture toughness in SA302B are shown in Figs. 15 and 16.

It is apparent from Figs. 12 to 16 that the RKR critical cleavage stress model[4] provides a very good description of lower shelf toughness behavior in these steels for temperatures up to NDTT, although experimental data for SA302B are extremely sparse. Above the NDT temperature, however, RKR predictions tend to level off, due to the smaller temperature variation

*The hardening exponent n is defined here in terms of the usual constitutive law $\sigma/\sigma_o = (\epsilon_p/\epsilon_o)^n$. This corresponds to a hardening exponent of $N = 1/n$ in terms of the Ramberg-Osgood law used in the HRR solution (Eqs. [1] to [3]).

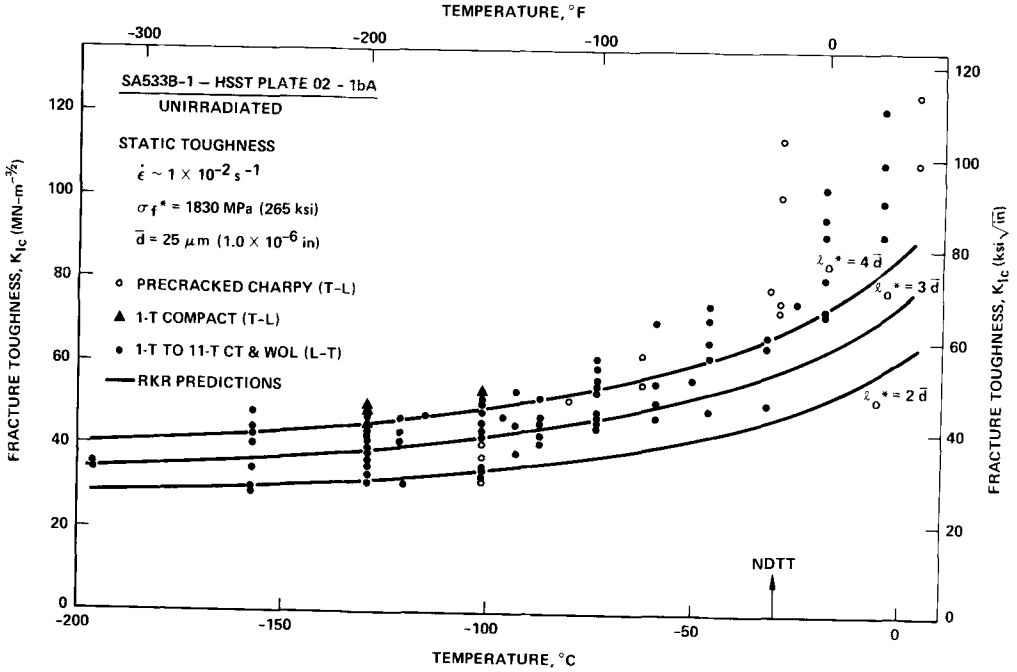

Fig. 12–Comparison of critical stress model (RKR) predictions with lower shelf static fracture toughness values for unirradiated SA533B-1.

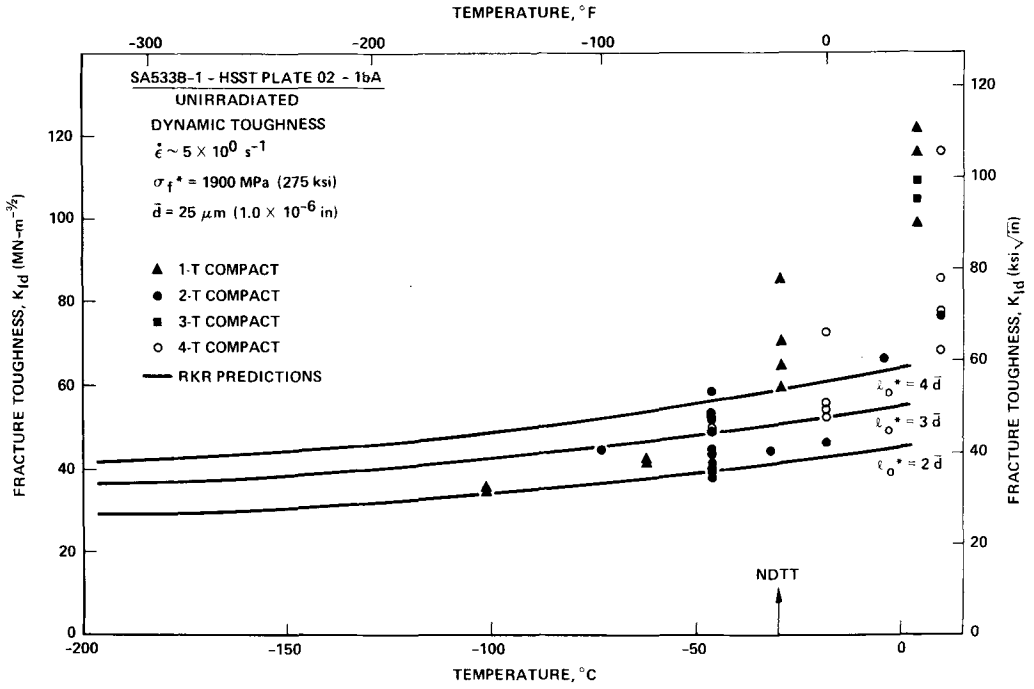

Fig. 13–Comparison of critical stress model (RKR) predictions with lower shelf dynamic compact fracture toughness values for unirradiated SA533B-1.

of yield strength, and markedly underestimate the data. As pointed out previously,[4] this is not to be unexpected since at temperatures above NDTT but below the upper shelf, failure in these steels can no longer be considered as unstable cleavage, and involves a transitional behavior of increasing amounts of ductile tearing between "stable" cleavage microcracks. Such failure is clearly not amenable to analysis using a purely critical stress model for failure.

Thus, lower shelf static and dynamic fracture toughness values in both SA533B-1 and SA302B are consistent with the attainment of a critical cleavage fracture stress over a distance of 2 to 4 prior austenite grain diameters ahead of the crack tip, at test temperatures below NDTT.

Upper Shelf Toughness

Unlike the critical stress model described above where the measured critical fracture stress (σ_f^*) is assumed to be effectively independent of temperature, use of the critical strain model to predict upper shelf toughness requires determination of the critical fracture strain ($\bar{\epsilon}_f^*$) at each temperature in question. Due to availability of specimens, values of $\bar{\epsilon}_f^*$ were only determined at three upper shelf temperatures (24, 71, and 177°C) at a single strain-rate ($\dot{\epsilon} \simeq 10^{-2}\ s^{-1}$).

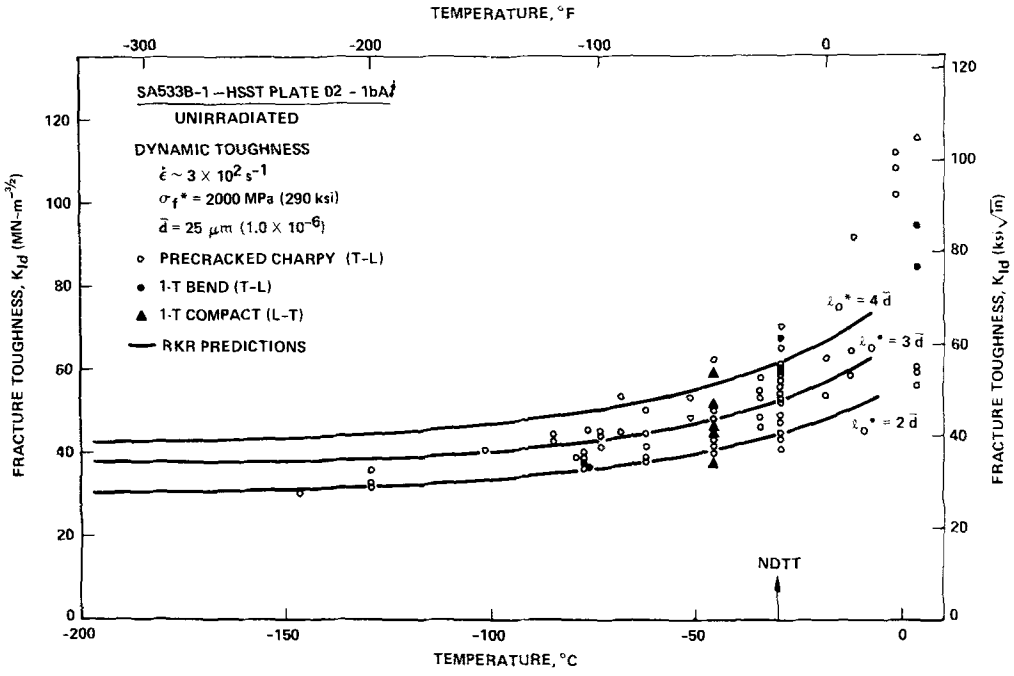

Fig. 14—Comparison of critical stress model (RKR) predictions with lower shelf dynamic (impact) fracture toughness values for unirradiated SA533B-1.

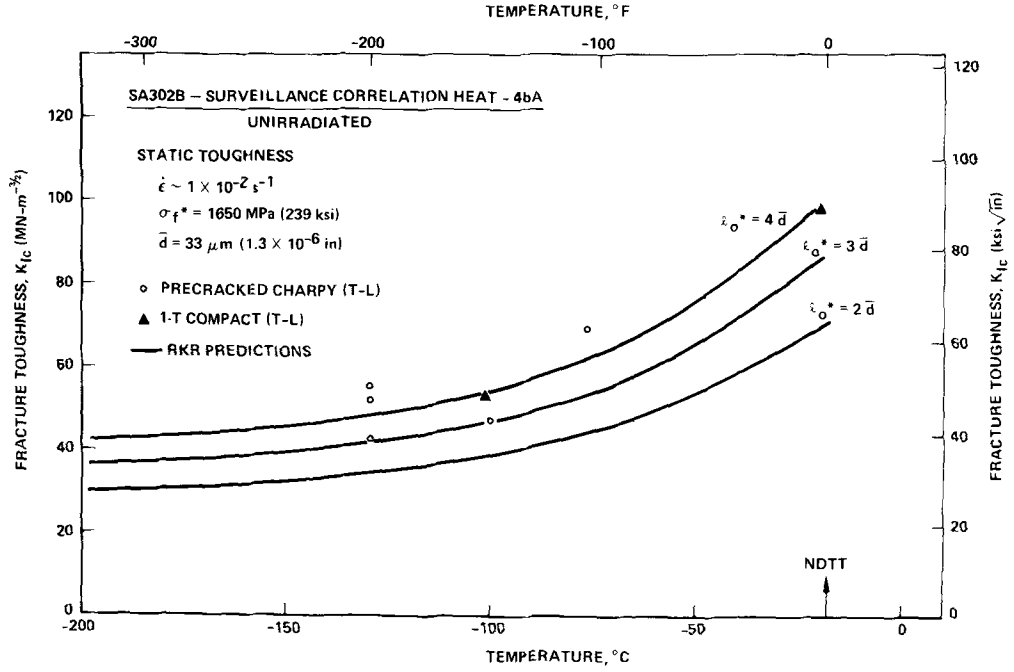

Fig. 15—Comparison of critical stress model (RKR) predictions with lower shelf static fracture toughness values for unirradiated SA302B.

Furthermore, valid fracture toughness data, computed from initiation J_{IC} values, in this temperature range are somewhat rare. However, using the fracture strain as a function of stress state data (Figs. 7 to 9) and the Rice and Johnson near-tip strain distribution[14] (Fig. 3), predictions of the upper shelf static fracture toughness between room temperature and 200°C for both steels were made using the critical fracture strain model. Results for unirradiated SA533B-1, and SA302B are illustrated in Figs. 17 and 18, respectively. For SA533B-1, the experimental data are best described by the attainment of a critical fracture strain ($\overline{\epsilon}_f^*$) over a characteristic distance (l_o^*) of 300 to 350 μm ahead of the crack tip (Fig. 17) whereas in SA302B, l_o^* is of the order of 100 to 150 μm. The significantly lower upper shelf toughness of SA302B is thus consistent with a lower plane strain ductility and a smaller characteristic distance.

Several points are worthy of note from these critical strain fracture toughness predictions for the upper shelf. First, it is apparent that over this temperature range, critical fracture strains ($\overline{\epsilon}_f$) at highly triaxial stress states ($\sigma_m/\overline{\sigma} > 1.2$), representative of the near-tip region, only marginally decrease with increasing temperature (Figs. 7 to 9). Furthermore, since the yield strength (σ_y) shows only a slight temperature dependence (*e.g.*, Fig. 5), the critical strain model predicts an essentially constant fracture toughness at the upper shelf (see Eq. [10]), consistent with most experimental data.[37,43-45]

Second, the critical microstructural size scales (l_o^*) for ductile fracture in SA302B and SA533B-1 are

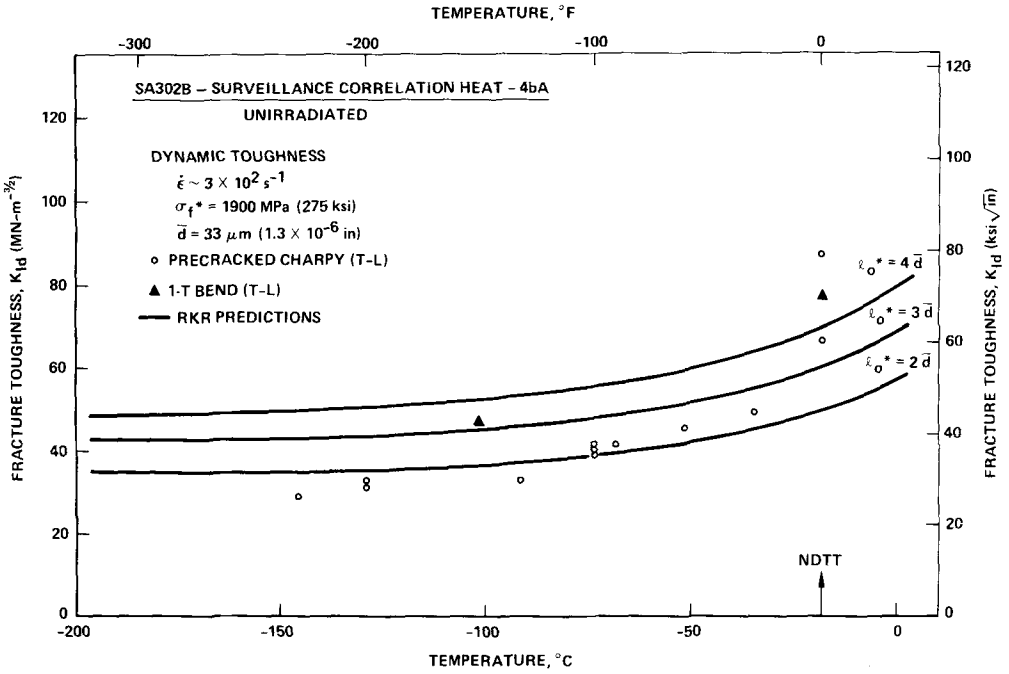

Fig. 16—Comparison of critical stress model (RKR) predictions with lower shelf dynamic (impact) fracture toughness values for unirradiated SA302B.

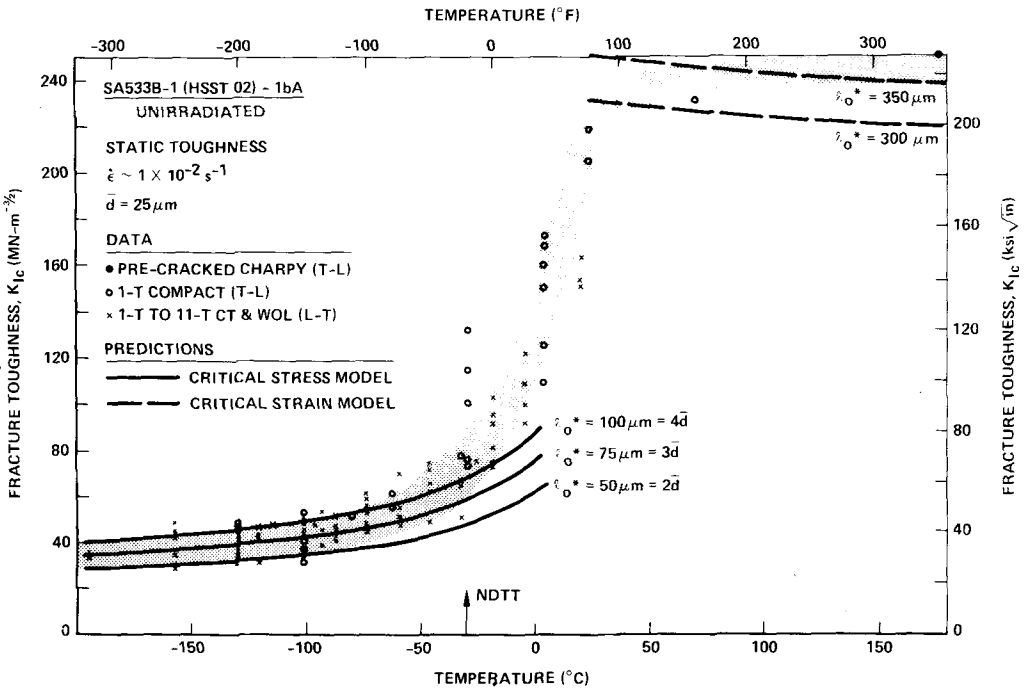

Fig. 17—Variation of static fracture toughness (K_{Ic}) with temperature for unirradiated SA533B-1, showing comparison of experimental data with critical stress and critical strain model predictions.

of the order of 1 and 6 to 7 times the planar inter-inclusion spacing, respectively. On the assumption that the critical event for the initiation of ductile fracture is the coalescence of major voids, formed at inclusions, to the main crack tip, this infers that it is the coalescence of a single major void to the crack tip which is critical for fracture in SA302B, whereas in SA533B-1 the coalescence of several major voids within the plastic zone is required. The latter fact is entirely consistent with the fractographic studies on SA533B-1,[3] which showed that the crack growth mechanism was not simply the nucleation of one void which coalesced with the main crack, but rather the nucleation and linkage of several isolated voids within the plastic zone. Similar conclusions have been reported for ductile fracture in other low strength steels.[31] Thus, for ductile fracture, the characteristic distance must be regarded as not merely reflecting the spacing between particles which nucleate major voids, but also the critical number of voids which coalesce with the main crack at the initiation of crack growth.

Hence, application of the critical strain model for upper shelf ductile fracture indicates that static fracture toughness values for crack initiation in SA302B are consistent with the attainment of a critical fracture strain (*i.e.*, the ductility at a highly triaxial stress-state) over a distance of roughly one inclusion spacing from the crack tip. In SA533B-1, however, crack initiation is consistent with the attainment of a critical fracture strain over several inclusion spacings, infer-

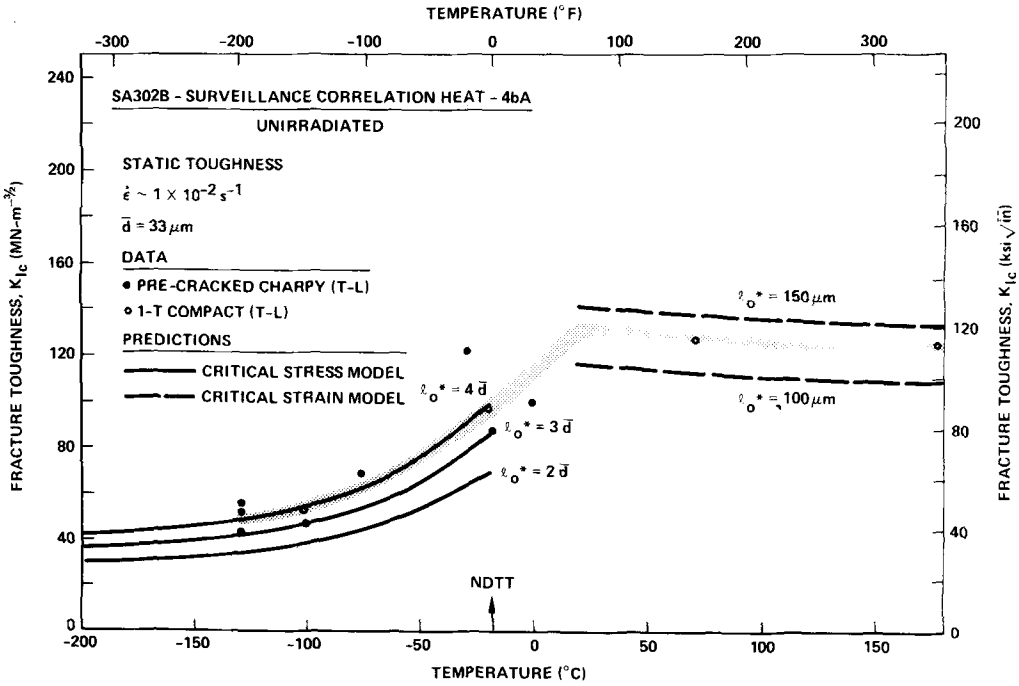

Fig. 18—Variation of static fracture toughness (K_{Ic}) with temperature for unirradiated SA302B, showing comparison of experimental data with critical stress and critical strain model predictions.

ring that the critical fracture event involves the coalescence of more than one major void to the crack tip.

INFLUENCE OF NEUTRON IRRADIATION

Neutron irradiation embrittlement of nuclear pressure vessel steels is generally characterized by an increase in the Charpy V-notch transition temperature (DBTT) and a drop in the Charpy V-notch upper shelf energy (Fig. 1), corresponding, in fracture mechanics terms, to a decrease in the fracture toughness K_{Ic}. An eventual aim of the present studies was to use the critical fracture models described to predict this decrease in toughness in SA533B-1 and SA302B as a function of neutron fluence. Due to the lack of available data, this has proved possible only for lower shelf K_{Ic} measurements in irradiated SA533B-1.

The work of Parks[7] first showed the applicability of the RKR critical cleavage stress model[4] for the prediction of irradiated toughness at the lower shelf. Neutron irradiation is assumed to increase the yield strength[36-38] and reduce the work hardening exponent,[46] while leaving the critical fracture stress for cleavage (σ_f^*) unchanged. The characteristic distance is also considered unaltered by irradiation, since grain size and particle spacings will remain the same. Thus by merely utilizing the effects of irradiation on yield and flow properties, the temperature dependence of lower shelf fracture toughness as a function of neutron fluence can be quantitatively evaluated using the RKR model, calibrated on unirradiated material.

Valid low temperature static fracture toughness data for unirradiated and irradiated SA533B-1 is shown in Fig. 19. Irradiated data are shown for neutron fluences of 1.2 to 1.3,[36] 2.2 to 4.2,[36,37,44] and 7.7 to 8.3 × 10^{19} n/cm^2,[38,39] $E > 1$ MeV, at irradiation temperatures between 265 and 297°C. Utilizing the RKR criterion for cleavage fracture in that the critical fracture stress, measured in unirradiated steel (σ_f^* = 1830 MPa), is attained over a characteristic distance of 3 grain diameters ($l_o^* = 3\bar{d}$), predictions for the temperature dependence of K_{Ic} for these fluences* were made, using irradiated yield stress data,[36-38,40,43,44] corrected for a crack tip strain rate of approximately $10^{-2}\ s^{-1}$, and a work hardening exponent of $n = 0$ ($N = \infty$). These predictions are shown by the curves in Fig. 19. It is clear that the critical stress model correctly predicts the shift in toughness curve to higher temperatures with increasing radiation, and closely reproduces the available experimental data.

*This represents a wider range of neutron fluences than was first analyzed by Parks.[7]

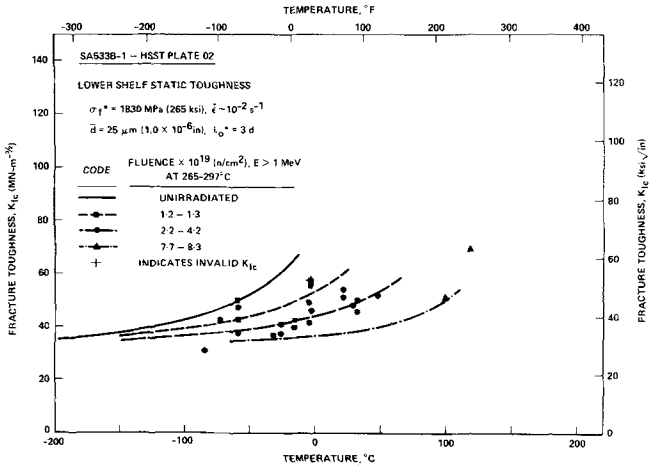

Fig. 19—Critical stress model (RKR) predictions of radiation effects on lower shelf fracture toughness compared with experimental data on neutron irradiated SA533B-1.

Similar procedures to predict the influence of neutron irradiation on upper shelf toughness using the critical strain model are plausible in theory, but are limited at present by the absence of data for the variation of fracture ductility with stress state in irradiated steel. Also, reliable initiation J_{Ic} fracture toughness data at

upper shelf temperatures are still unavailable. Moreover, some concern might be raised over the procedure of using a characteristic distance for irradiated steel determined from unirradiated data (*cf.* critical stress model). Since it appears that the characteristic distance for ductile fracture may be a function both of the microstructure (*i.e.*, the inter-inclusion spacing) and of the average number of voids which coalesce with the crack tip at crack initiation, it is by no means certain that the same number of voids will be involved at fracture initiation in irradiated steel. This is simply because the reduced strain hardening capacity of irradiated material will result in earlier coalescence by plastic shear localization of major voids. Thus, the feasibility of using the critical strain model for predicting upper shelf irradiated fracture toughness *cannot* be tested at present, and must await reliable information for the critical fracture strains and initiation J_{Ic} values for irradiated steel.

SUMMARY AND CONCLUSIONS

The present work has examined the application of simple fracture models to predict the temperature variation of plane strain fracture toughness in unirradiated and irradiated nuclear pressure vessel steels. These models attempt to combine accurate continuum mechanics solutions for the stress and strain distributions ahead of crack tips with necessarily simplified idealizations of the microscopic fracture mechanisms involved. For lower shelf cleavage fracture at low temperatures below NDTT, fracture toughness values, under both quasi-static and dynamic loading in SA533B-1 and SA302B steels, are consistent with the attainment of a critical fracture stress over a distance of 2 to 4 prior austenite grain diameters ahead of the crack tip, according to the RKR critical stress model for slip-initiated cleavage. Further, the influence of neutron irradiation on fracture toughness at these temperatures can be closely predicted by this model, assuming that the critical fracture stress and microstructurally significant characteristic distance are unchanged, and that the decrease in toughness with increasing fluence results from the effect of irradiation on yield and flow properties.

Similarly, for upper shelf ductile fracture at temperatures between ambient and 200°C, elastic-plastic initiation fracture toughness values under quasi-static loading in unirradiated SA533B-1 and SA302B are consistent with the attainment of a critical fracture strain (determined for highly triaxial stress states) over a characteristic distance related to the major inclusion spacing, according to the critical stress modified strain model for microvoid coalescence. The characteristic dimension in the latter case appears to depend both on the microstructure (*i.e.*, particle spacing) and the number of major voids which coalesce with the main crack tip at fracture initiation.

Whilst it is felt that *a priori* predictions of macroscopic fracture behavior (*i.e.*, fracture toughness values) using such models for local failure criteria are not at present feasible because of uncertainties in the magnitude of the microstructurally significant dimension, the description of fracture toughness in terms of these models does provide insight into the micromechanics and mechanisms of failure, and furthermore provides a vital connection between continuum plasticity and microstructural mechanisms of fracture.

ACKNOWLEDGMENTS

The work was performed under Contract No. RP886-1 from the Electric Power Research Institute, Palo Alto, California. Thanks are due to Dr. John Bassani for his critical review of the manuscript.

REFERENCES

1. Reports of the United States Atomic Energy Commission Heavy Section Steel Technology (HSST) Program, HSST Technical Reports no. 1-36, 1968-1975.
2. R. A. Wullaert, J. W. Scheckherd, and R. W. Smith: ASTM STP 611, ASTM, pp. 400-17, 1976.
3. R. H. Van Stone: General Electric Report no. SRD-78-116 for EPRI, pp. 5.1-5.13, General Electric Company, Schenectady, NY, July, 1978.
4. R. O. Ritchie, J. F. Knott, and J. R. Rice: *J. Mech. Phys. Solids,* 1973, vol. 21, pp. 395-410.
5. F. A. McClintock: *Fracture, An Advanced Treatise,* H. Leibowitz, ed., vol. 3, pp. 47-225, Academic Press, NY, 1971.
6. A. C. MacKensie, J. W. Hancock, and D. K. Brown: *Eng. Fract. Mech.,* 1977, vol. 9, pp. 167-88.
7. D. M. Parks: *J. Eng. Mater. Technol.,* Ser. H, 1976, vol. 98, pp. 30-35.
8. E. Orowan: *Rep. Prog. Phys.,* 1948, vol. 12, p. 185.
9. J. F. Knott: *J. Iron Steel Inst.,* 1966, vol. 204, pp. 104-11.
10. J. W. Hutchinson: *J. Mech. Phys. Solids,* 1968, vol. 16, pp. 13-31.
11. J. R. Rice and G. F. Rosengren: *Ibid.,* pp. 1-12.
12. J. R. Rice and D. M. Tracey: *Numerical and Computational Methods in Structural Mechanics,* S. J. Fenves *et al.,* eds., Academic Press, NY, 1973.
13. D. M. Tracey: *J. Eng. Mater. Technol.,* Series H, 1976, vol. 98, pp. 146-51.
14. J. R. Rice and M. A. Johnson: *Inelastic Behavior of Solids,* M. F. Kanninen *et al.,* eds., p. 641, McGraw Hill, NY, 1970.
15. R. M. McMeeking: *J. Eng. Mater. Technol.,* Series H, 1976, vol. 98, pp. 146-51.
16. S. P. Rawal and J. Gurland: *Met. Trans. A,* 1977, vol. 8A, pp. 691-98.
17. D. A. Curry and J. F. Knott: *Met. Sci.,* 1976, vol. 10, pp. 1-6.
18. D. A. Curry: C.E.R.L. Technical Report No. RD/L/N 64/78, Central Electricity Research Laboratory, Leatherhead, England, 1978.
19. H. J. Rack: *Mater. Sci. Eng.,* 1976, vol. 24, pp. 165-70.
20. J. R. Rice: *J. Appl. Mech.,* Ser. E, 1968, vol. 35, p. 379.
21. T. R. Wilshaw, C. A. Rau, and A. S. Tetelman: *Eng. Fract. Mech.,* 1968, vol. 1, pp. 191-211.
22. A. S. Tetelman, T. R. Wilshaw, and C. A. Rau: *Int. J. Fract. Mech.,* 1968, vol. 4, p. 147.
23. R. Hill: *The Mathematical Theory of Plasticity,* Oxford University Press, 1950.
24. A. P. Green and B. B. Hundy: *J. Mech. Phys. Solids,* 1956, vol. 4, pp. 128-44.
25. J. R. Griffiths and D. R. J. Owen: *Ibid.,* 1971, vol. 19, pp. 419-31.
26. D. R. J. Owen, G. C. Nayak, A. P. Kfouri, and J. R. Griffiths: *Int. J. Num. Methods Eng.,* vol. 6, 1973, p. 63.
27. J. W. Hancock and A. C. MacKenzie: *J. Mech. Phys. Solids,* 1976, vol. 24, pp. 147-69.
28. R. O. Ritchie and R. M. Horn: *Met. Trans. A.,* 1978, vol. 9A, pp. 331-44.
29. P. W. Bridgman: *Studies in Large Plastic Flow and Fracture,* McGraw Hill, 1952.
30. R. M. McMeeking: *J. Mech. Phys. Solids,* 1977, vol. 25, pp. 357-81.
31. R. K. Pandey and S. Banerjee: *Eng. Fract. Mech.,* 1978, vol. 10, pp. 817-29.
32. J. R. Hester and C. R. Brooks: *Proceedings of Heavy Section Steel Technology Program,* Fourth Annual Information Meeting, Oak Ridge National Laboratory, March/April 1970.
33. W. L. Server and W. Oldfield: EPRI Report no. NP-933, Electric Power Research Institute, Palo Alto, CA, December 1978.
34. J. D. Landes and J. A. Begley: Westinghouse Scientific Paper 76-1E7-JTINTF-P3, Westinghouse Scientific Laboratories, Pittsburgh, PA, May, 1976.
35. W. O. Shabbits: HSST Technical Report no. 13, Westinghouse Electric Corp., Pittsburgh, PA, December, 1970.
36. J. R. Mager and F. O. Thomas: HSST Technical Report no. 5, Westinghouse Electric Corp., Pittsburgh, PA, November, 1969.
37. G. W. Hunter and J. A. Williams: *Nuc. Eng. Des.,* 1971, vol. 17, pp. 131-48.
38. J. A. Williams: HSST Technical Report no. 31, Hanford Engineering Development Laboratory, Richland, WA, 1973.
39. W. Oldfield, R. A. Wullaert, W. L. Server, and T. R. Wilshaw: ETI Technical Report no. TR75-34R, Effects Technology, Inc., Santa Barbara, CA, July, 1975.
40. J. M. Steichen and J. A. Williams: HSST Technical Report no. 32, Hanford Engineering Development Laboratory, Richland, WA, July, 1973.

41. W. L. Server: *J. Eng. Mater. Technol.*, Ser. H, 1978, vol. 100, pp. 183-88.
42. P. E. Bennett and G. M. Sinclair: *J. Basic Eng.*, Ser. D, 1966, vol. 88, pp. 518-24.
43. J. A. Williams: HSST Technical Report no. 36, Hanford Engineering Development Laboratory, Richland, WA, January, 1975.
44. G. D. Whitman: *Proc. Fourth Water Reactor Safety Research Information Meeting*, (sponsored by Office of Water Reactor Safety Research, Nuclear Regulatory Commission). Gaithersburg, Maryland, September 1976.
45. W. L. Server: ASTM STP 668, ASTM, pp. 493-514, 1979.
46. N. Igata, H. Kayano, and K. Watanabe: ASTM STP 570, ASTM, pp. 24-37,1975.